Supporting information

Generating green hydrogen via nickel sulfide modified titania thin film photocatalysts

Melissa Sophie Egger,[a] Stephen Nagaraju Myakala,[b] Marco Sigl,[a] Georg Haberfehlner,[c] Manfred Nachtnebel,[d] Anto Vrbat,[e] Thomas Griesser,[e] Alaaddin Cem Ok,[b,f] Alexey Cherevan,[b] Dominik Eder,[b] Thomas Rath,[a,*] Gregor Trimmel[a,*]

[a] Institute for Chemistry and Technology of Materials (ICTM), NAWI Graz, Graz University of Technology, Stremayrgasse 9, 8010 Graz, Austria

[b] Institute of Materials Chemistry, Technical University Vienna, Getreidemarkt 9, 1060 Vienna, Austria

[c] Institute of Electron Microscopy and Nanoanalysis (FELMI), Graz University of Technology, Steyrergasse 17, 8010 Graz, Austria

[d] Graz Centre for Electron Microscopy (ZFE), Steyrergasse 17, 8010 Graz, Austria

[e] Institute of Chemistry of Polymeric Materials, Montanuniversität Leoben, Otto-Glöckel-Straße 2, 8700 Leoben, Austria

[f] Department of Metallurgical and Materials Engineering, Faculty of Engineering, Marmara University, TR-34722 Istanbul, Turkey

* Corresponding author email address: gregor.trimmel@tugraz.at, thomas.rath@tugraz.at

X-Ray diffraction (XRD)

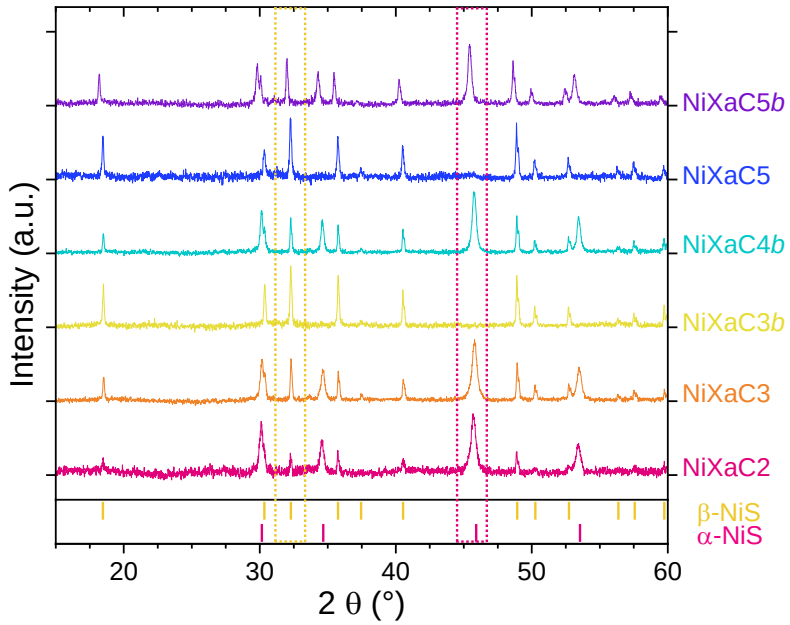

Figure S1 XRD diffractograms of NiS thin films sintered at 400°C

Scanning transmission electron microscopy (STEM)

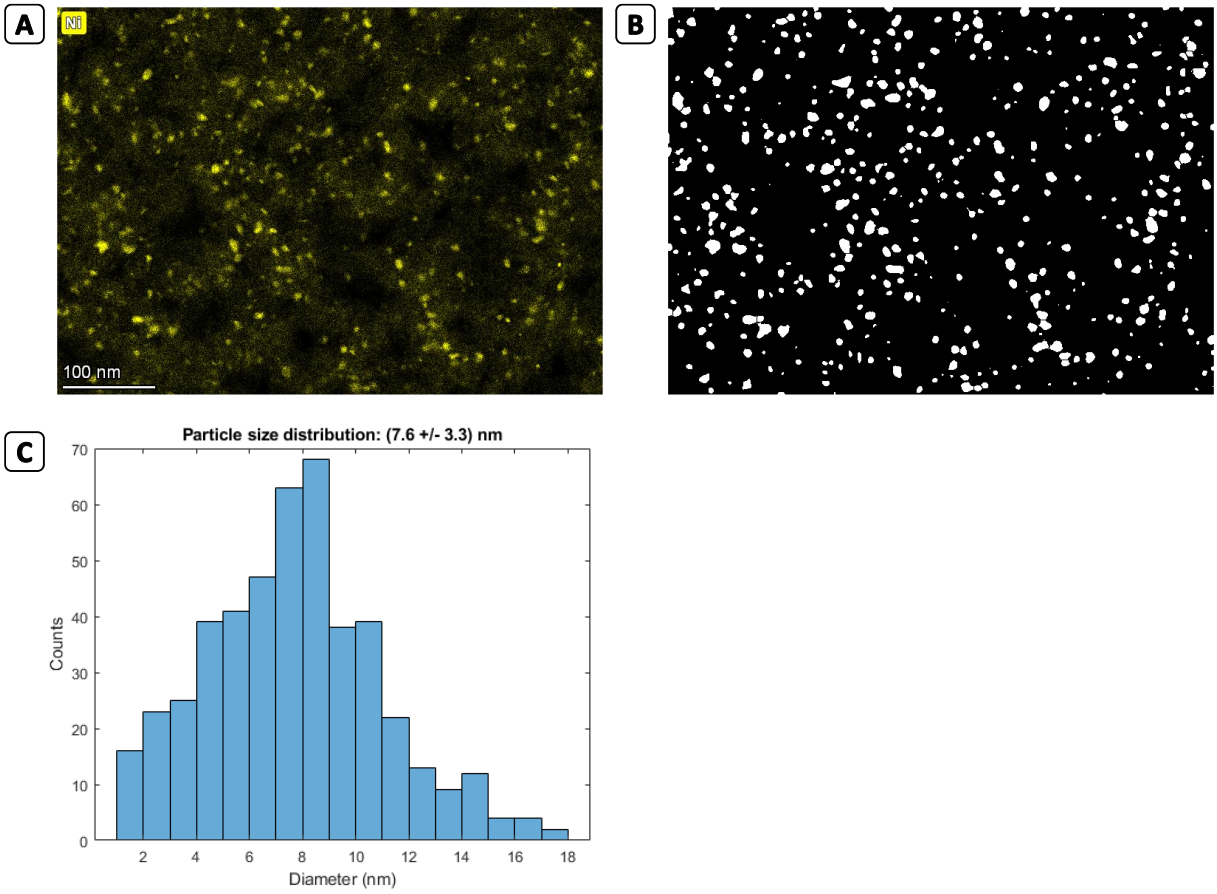

Figure S2 Particle size distribution for nickel sulfide. (A) EDS elemental map of nickel. (B) segmentation of the nickel map. (C) particle size distrbution.

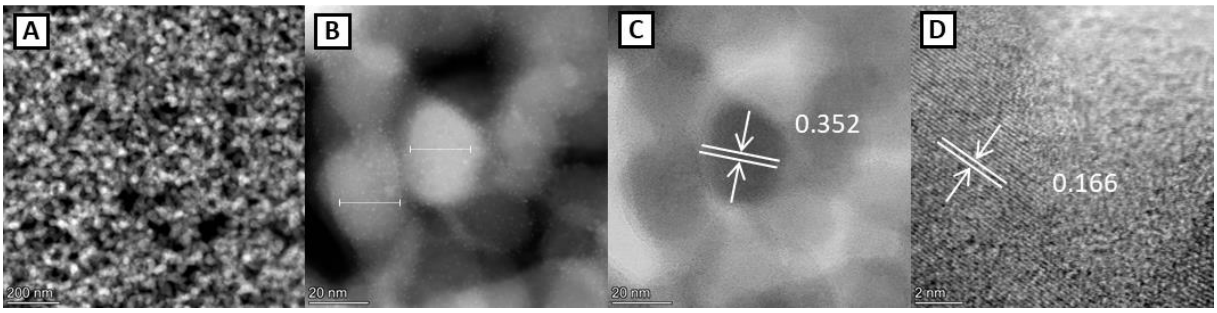

Figure S3 (A, B): HAADF-STEM images of the sample cross section at two different magnifications. In (B), crystallites in the range of approximately 25 nm can be observed. The small, bright spots located on the surface of the titania particles are small atomic clusters of Pt, which stem from redeposition of the Pt used in the sample preparation. (C, D): BF images at two different magnifications with the interplanar spacings of the observed anatase ((101), 0.352 nm) and ((105), 0.166 nm) planes marked.

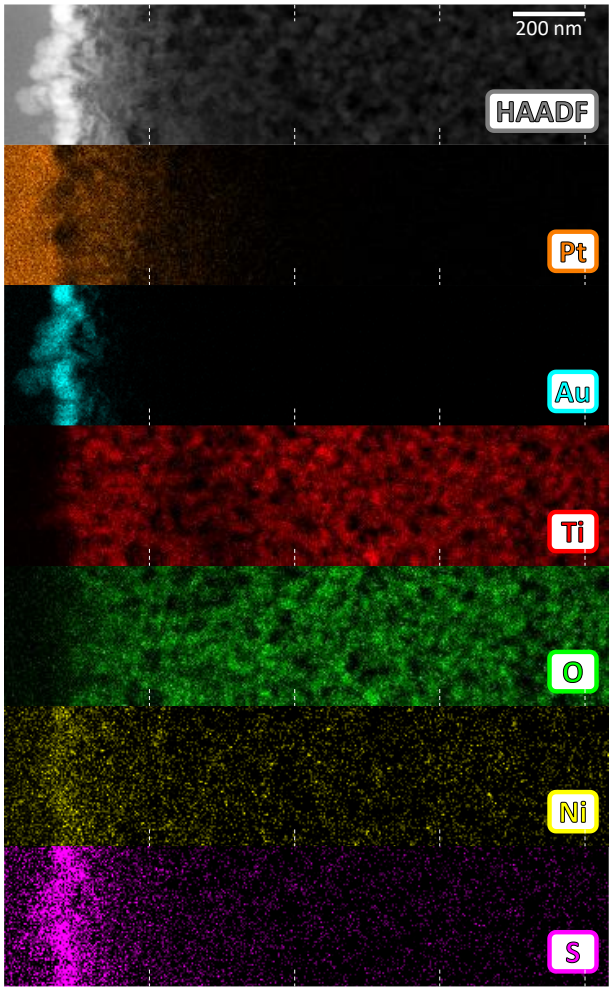

Figure S4 HAADF-STEM image and EDS elemental maps of the sample cross-section starting at the protection layer of gold and platinum on the sample surface. Platinum (orange), gold (light blue), titanium (red), oxygen (green), nickel (yellow), sulfur (pink)

The area of the elemental mapping (Figure S4, area indicated by a rectangle in Figure4A in the main manuscript) shows the region from the sample surface to approx. 1 µm inside the film.

UV-Vis: Titania film thickness determination

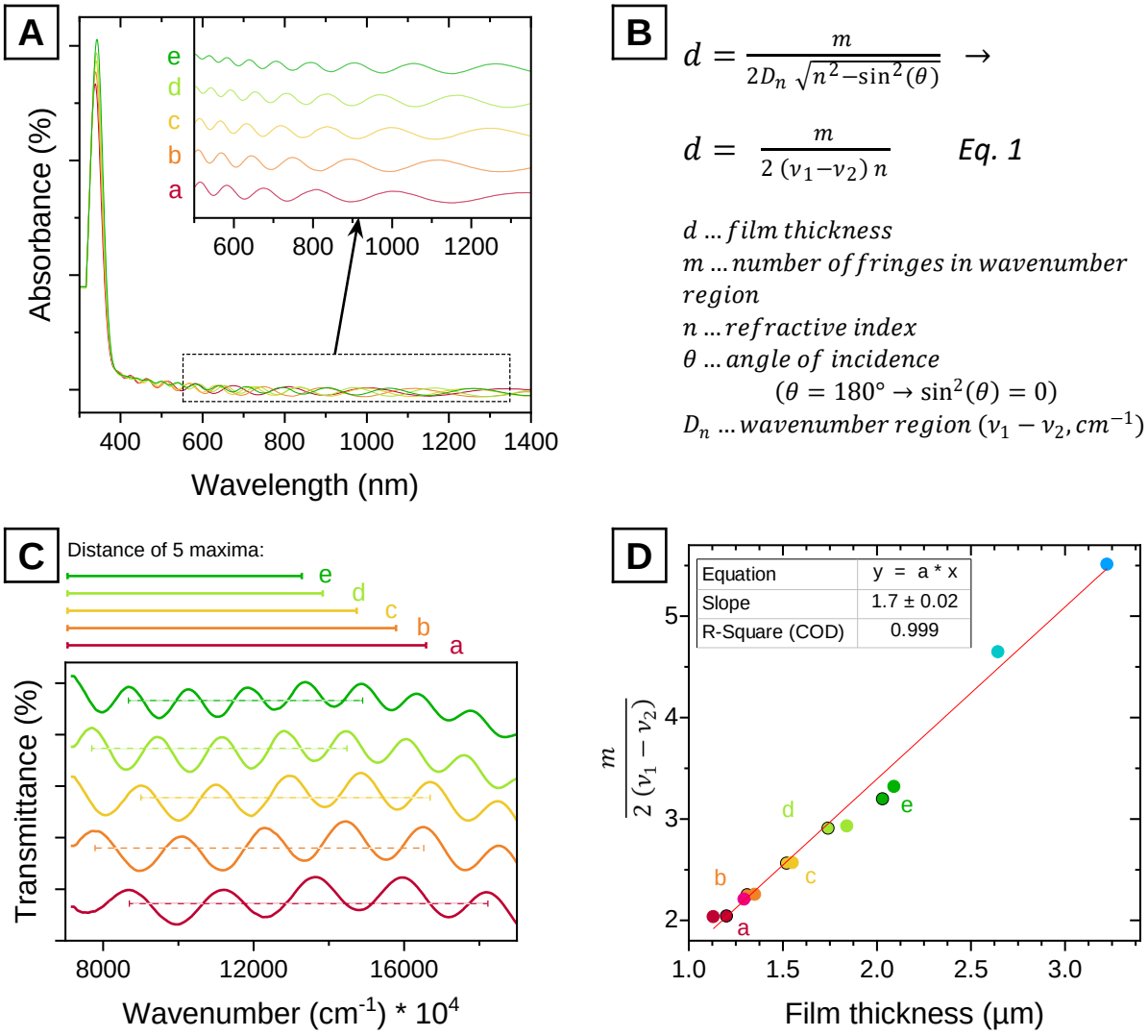

Figure S5 Film thickness determination of mesoporous titania thin films via UV-Vis and profilometry. The thickness of titania samples was varied by adjusting the spin coating speed and the number of layers. (A) Absorbance of 5 titania thin films with different film thicknesses (film thickness: a < b < c < d < d). Inset: Magnification of the region between 500 and 1300 nm showing the interference fringes resulting from a partially reflecting thin film on a reflecting substrate. (B) Equation giving the correlation between film thickness and refractive index.[1] (C) Transmittance vs wavenumber in the interference fringe region. (D) Film thickness (determined by profilometry) vs values calculated from eq. 1, showing a good linear correlation and yielding a refractive index of 1.7, which falls within the range of refractive indices reported for mesoporous titania (1.6 – 2.9).[2,3]

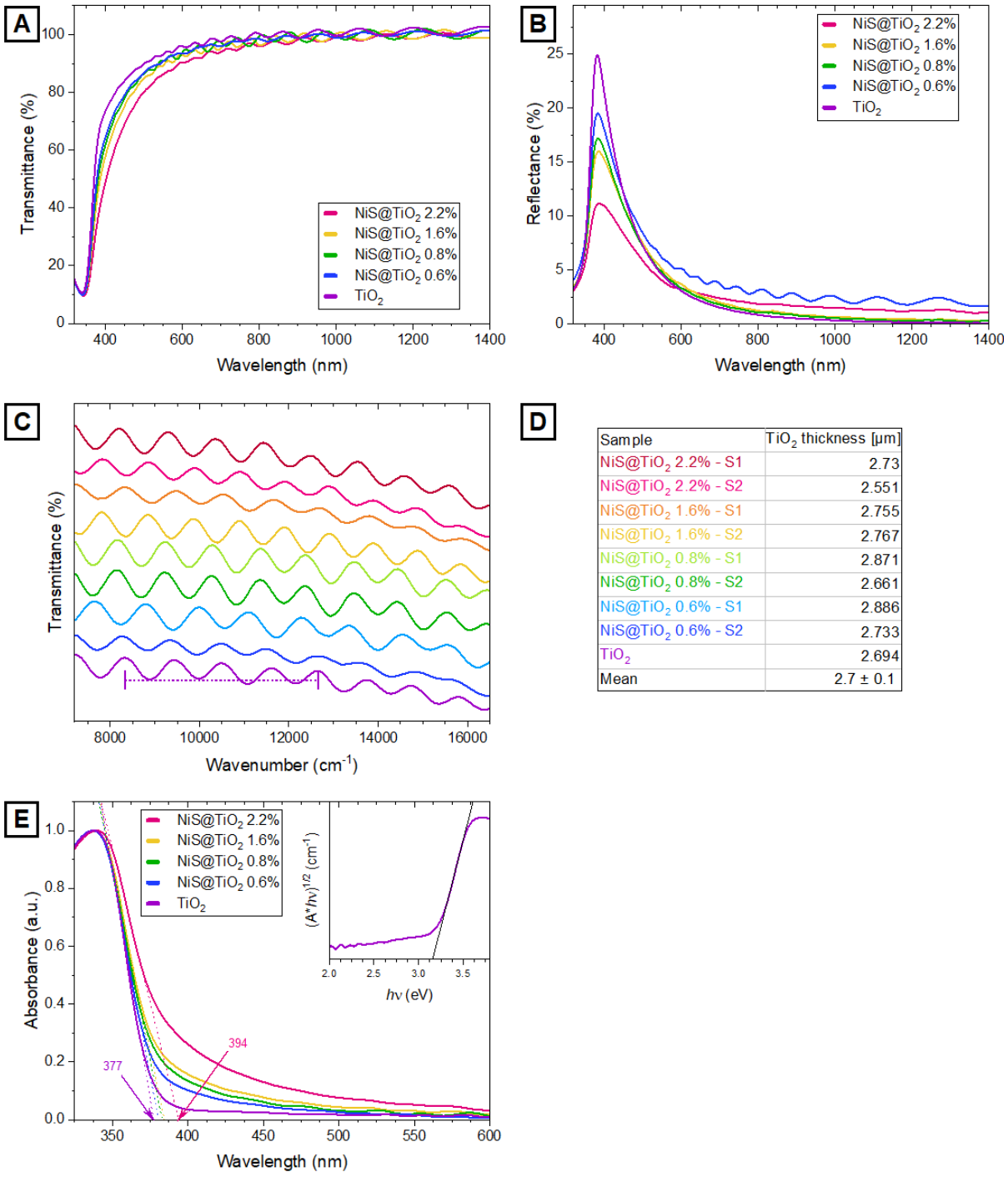

Sample	TiO_2 thickness [µm]
$NiS@TiO_2$ 2.2% - S1	2.73
$NiS@TiO_2$ 2.2% - S2	2.551
$NiS@TiO_2$ 1.6% - S1	2.755
$NiS@TiO_2$ 1.6% - S2	2.767
$NiS@TiO_2$ 0.8% - S1	2.871
$NiS@TiO_2$ 0.8% - S2	2.661
$NiS@TiO_2$ 0.6% - S1	2.886
$NiS@TiO_2$ 0.6% - S2	2.733
TiO_2	2.694
Mean	2.7 ± 0.1

Figure S6 Determination of the thickness of the titania film for the NiS-modified thin film titania samples by UV-Vis. (A) Transmittance and (B) diffuse reflectance spectra of $NiS@TiO_2$ thin films modified with four different amounts of NiS (c1 – pink, 2.2 ± 0.7 w%, c2 – yellow, 1.8 ± 0.6 w%, c3 – green, 0.8 ± 0.1 w%; c4 – blue, 0.6 ± 0.3 w%; purple: pure titania). (C) Transmittance vs wavenumber in the titania/glass interference fringe region. (D) Titania film thickness values calculated from the distance of the interference maxima, with a mean value of 2.74 ± 0.1 µm. (E) Normalized UV-Vis absorption spectra of $NiS@TiO_2$ thin films modified with different amounts of NiS. Inset: Tauc plot of the pristine titania film.

Determination of the NiS amount:

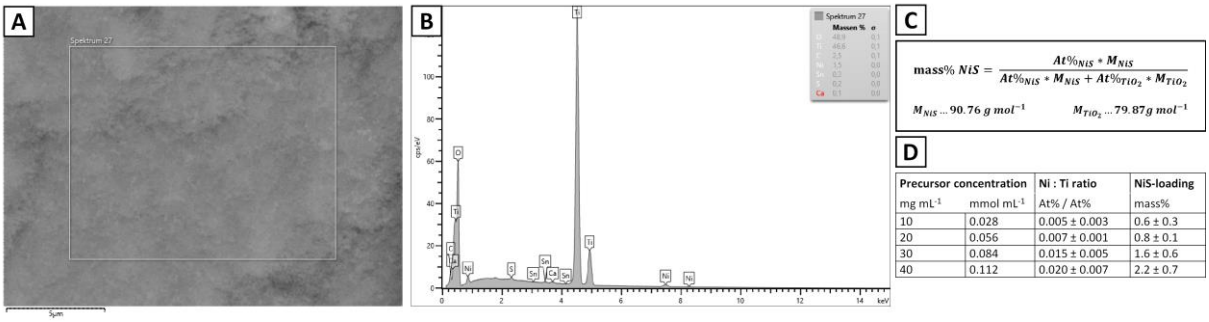

Precursor concentration		Ni : Ti ratio	NiS-loading
mg mL^{-1}	mmol mL^{-1}	At% / At%	mass%
10	0.028	0.005 ± 0.003	0.6 ± 0.3
20	0.056	0.007 ± 0.001	0.8 ± 0.1
30	0.084	0.015 ± 0.005	1.6 ± 0.6
40	0.112	0.020 ± 0.007	2.2 ± 0.7

Figure S7 Estimation of NiS amount on TiO_2 thin film catalyst using SEM-EDS: (A) SEM image and (B) corresponding EDS spectrum of a NiS@TiO_2 sample (precursor concentration: 0.112 mmol mL^{-1}). (C) Calculation of the NiS loading from the atomic percentages of Ni and Ti obtained by EDS. (D) Calculated NiS loadings for the precursor concentrations 0.028, 0.056, 0.084 and 0.112 mmol mL^{-1}. For each sample, the loading was calculated as the average of three EDS measurements.

Hydrogen evolution reaction (HER)

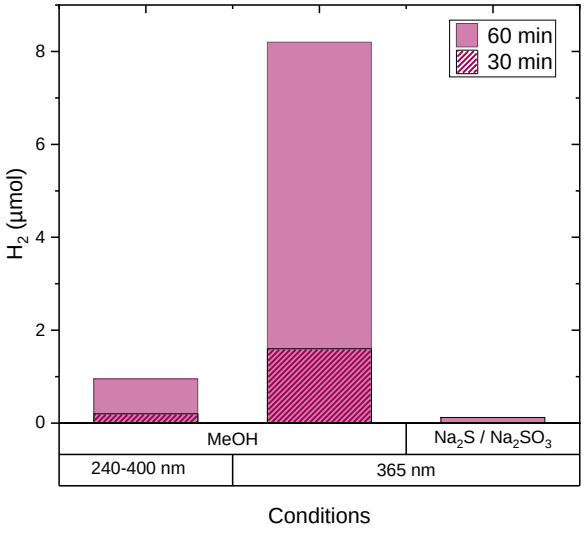

Figure S8 Evaluation of conditions for the hydrogen evolution reaction by varying light source, sacrificial reagent, and experiment time. Final experimental conditions: 240-400 nm light source, 50 v% MeOH, 60 minutes.

Table S1 Concentrations of precursor solutions for the preparation of the catalysts for the HER experiments.

Cocatalyst	Precursor solution (mg mL^{-1})	Precursor solution (mmol mL^{-1})	NiS:TiO_2 ◊ (mass%)	H_2 evolution (mmol h^{-1} g^{-1})
No cocatalyst				0.01
NiS (NiXaC4b)	5	0.014		1.09
NiS (NiXaC4b)	10	0.028	0.6 ± 0.3	0.89
NiS (NiXaC4b)	20	0.056	0.8 ± 0.1	2.35
NiS (NiXaC4b)	30	0.084	1.6 ± 0.6	2.27
NiS (NiXaC4b)	**40**	**0.112**	**2.2 ± 0.7**	**2.78**
NiS (NiXaC4b)	60	0.168		1.75
NiS (NiXaC4b)	60 (2 x coated)	Nominal precursor concentration: 0.336		0.67
NiS (NiXaC2)	25	0.084		2.00
NiS (NiXaC3)	28	0.084		2.02
NiS (NiXaC3b)	28	0.084		1.58
NiS (NiXaC5)	32	0.084		1.81
NiS (NiXaC5b)	32	0.084		2.28

◊Calculated from Ni:Ti (atom% : atom%) ratio determined via SEM-EDX (Figure S7)

The following HER measurements (Figure S9) were conducted in the process of manuscript revisions. By this point, we have optimized the cocatalyst deposition process by using longer infiltration times (10 s) and a higher solution volume to avoid higher cocatalyst concentrations on the surface. Also, the new batch of samples had an approximately 10% thicker titania layer. Therefore, we measured higher efficiencies for this batch.

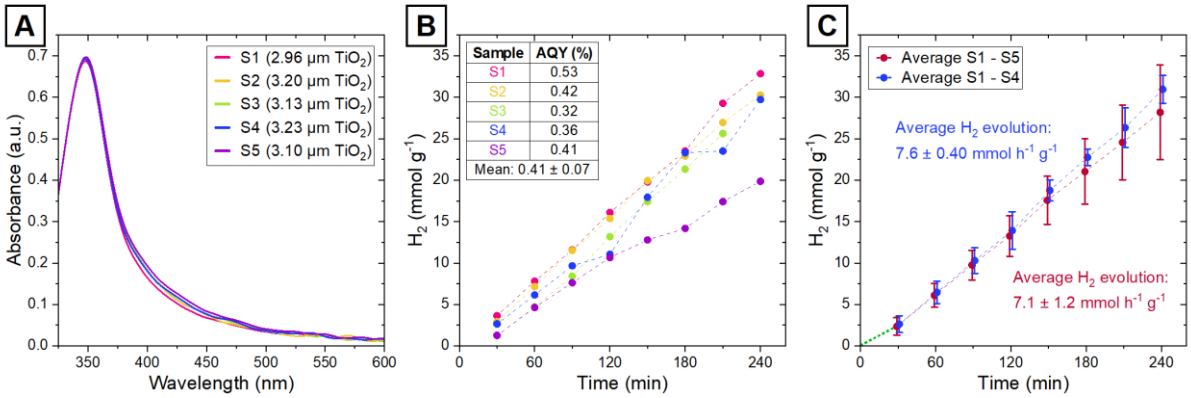

Figure S9 Multiple 4-h measurements of NiS@TiO_2 films with the best-performing cocatalyst loading (NiXaC4b precursor, 110 µmol mL^{-1}). (A) Absorption spectra for the five NiS@TiO_2 catalyst thin films, with the thickness of the titania calculated from the interference pattern. (B) HER measurements over four hours. For S3 (green), the last measurement point was excluded due to an instrumentation error. AQY values for each sample and the mean AQY (0.41 %) are given in the inset. (C) Hydrogen evolution averaged over all samples (red, 7.1 ± 1.2 mmol h^{-1} g^{-1}) and with the lowest-performing sample S5 (purple) excluded (blue, 7.6 ± 0.40 mmol h^{-1} g^{-1}). In the first 30 minutes, the hydrogen evolution rate was lower than the average (marked with a green dotted line). After that, the rate was approximately stable for the duration of the experiments. The overall experiment standard deviation for the average of S1-S4 was calculated as 14.5%.

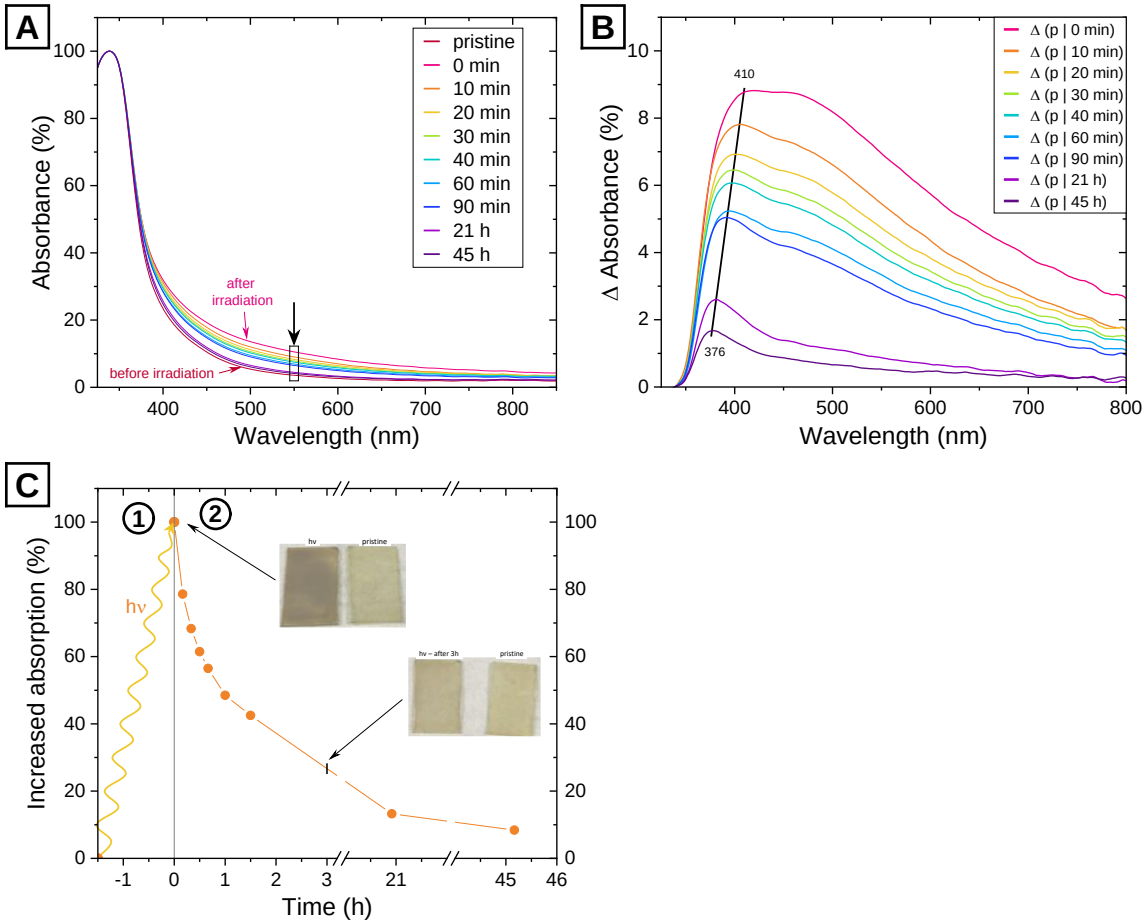

Figure S10 Reversible discoloration of the NiS@TiO_2 catalyst upon irradiation in 50 % MeOH (aq.). (A): UV-Vis Measurements of the catalyst before (pristine) irradiation, after 90 minutes with a Hg-vapor lamp at 2.5 W cm^{-1}, and at different times after irradiation. (B) Difference spectra: absorbance of the film at different times after irradiation (indicated with the time of measurement) – absorbance of the pristine film (indicated with p). (C) Increased absorption of the irradiated film compared to the pristine film (averaged over the wavelength range 545-555 nm). (1) 1 hour Illumination of the NiS@TiO_2 catalyst with a Mercury vapor lamp at 2.5 W cm^{-1} in 50 % aq. MeOH. (2) Decrease of the absorbance and pictures of the discolored film directly and 3 hours after illumination in comparison to a not illuminated film.

Cyclic voltammetry (CV)

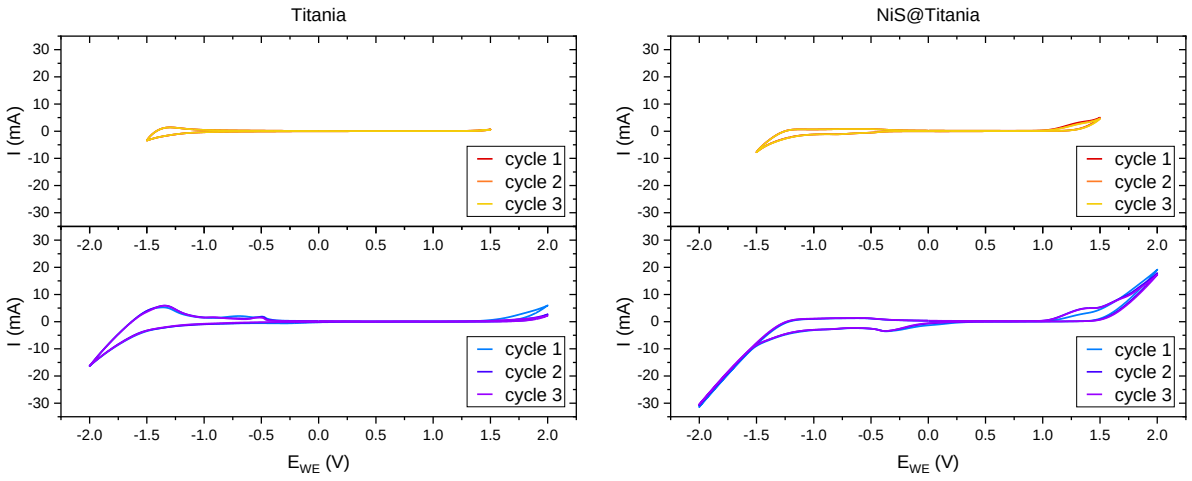

Figure S11 Cyclic voltammetry measurements of titania and Nis@TiO_2 films on FTO coated glass substrates. 1 M NaCl was used as electrolyte and purged for 10 minutes with nitrogen. The CV experiments were conducted with a scan rate of

50 mV s^{-1} between 1.5 and -1.5 V (upper row, red-yellow) and 2 and -2 V (lower row, blue-purple). No chemically irreversible change is observable in those regions.

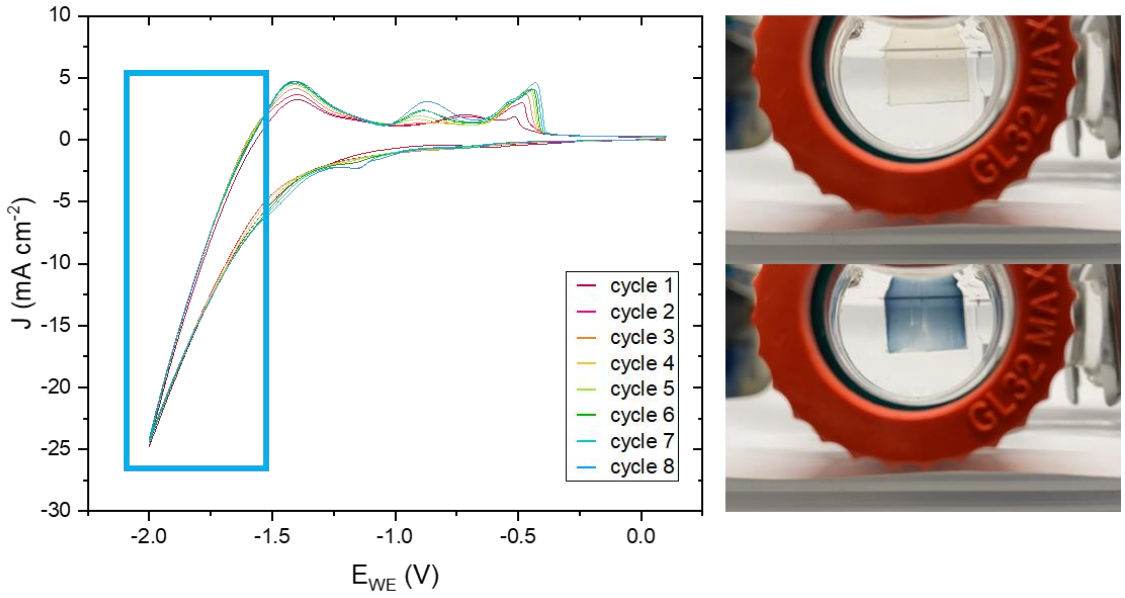

Figure S12 Cyclic voltammetry measurements of a TiO_2 film on FTO coated glass substrates. 1 M NaCl was used as electrolyte and purged for 10 minutes with nitrogen. For the experiment, a scan rate of 50 mV s^{-1} was used between 2 and -2 V for 8 cycles. The current density was calculated from the area of the film submerged in the electrolyte. Between -1.6 and -2 V a discoloration to a strong blue was observed, which completely disappeared again upon applying a more positive potential. This reversible discoloration can be attributed to self-doping of titania by the formation of Ti^{3+}.[4]

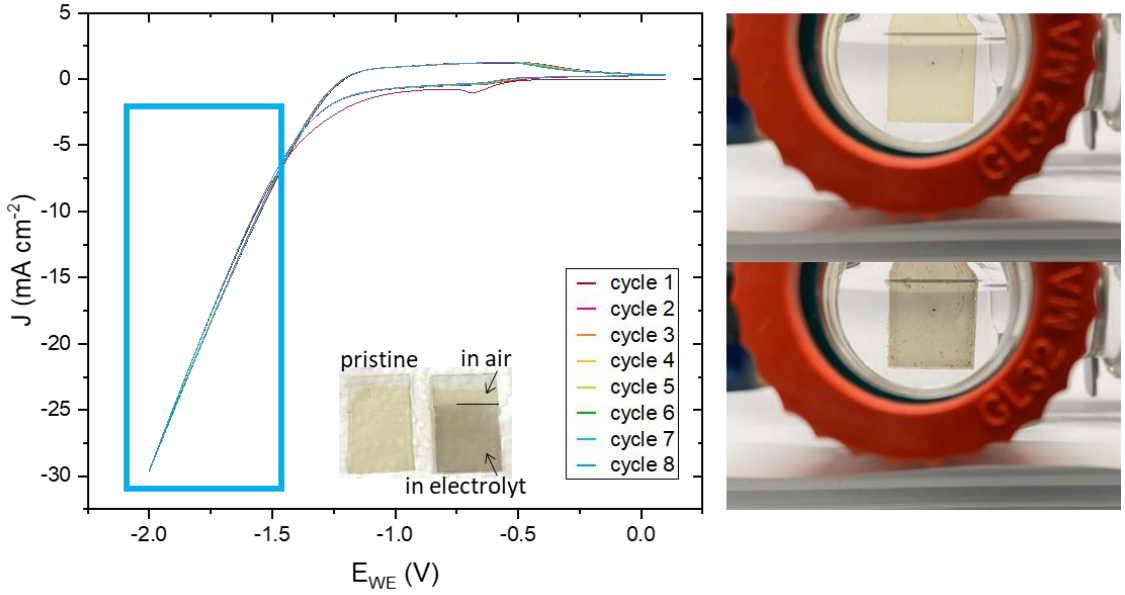

Figure S13 Cyclic voltammetry measurements of a NiS@TiO_2 film on FTO coated glass substrates. 1 M NaCl was used as electrolyte and purged for 10 minutes with nitrogen. For the experiment, a scan rate of 50 mV s^{-1} was used between 2 and -2 V for 8 cycles. The current density was calculated from the area of the film submerged in the electrolyte. Between -1.5 and -2 V a slight darkening of the film followed by the evolution of gas bubbles was observed. The discoloration returned to the previous color again upon applying a more positive potential. No degradation could be observed during the duration of the experiment.

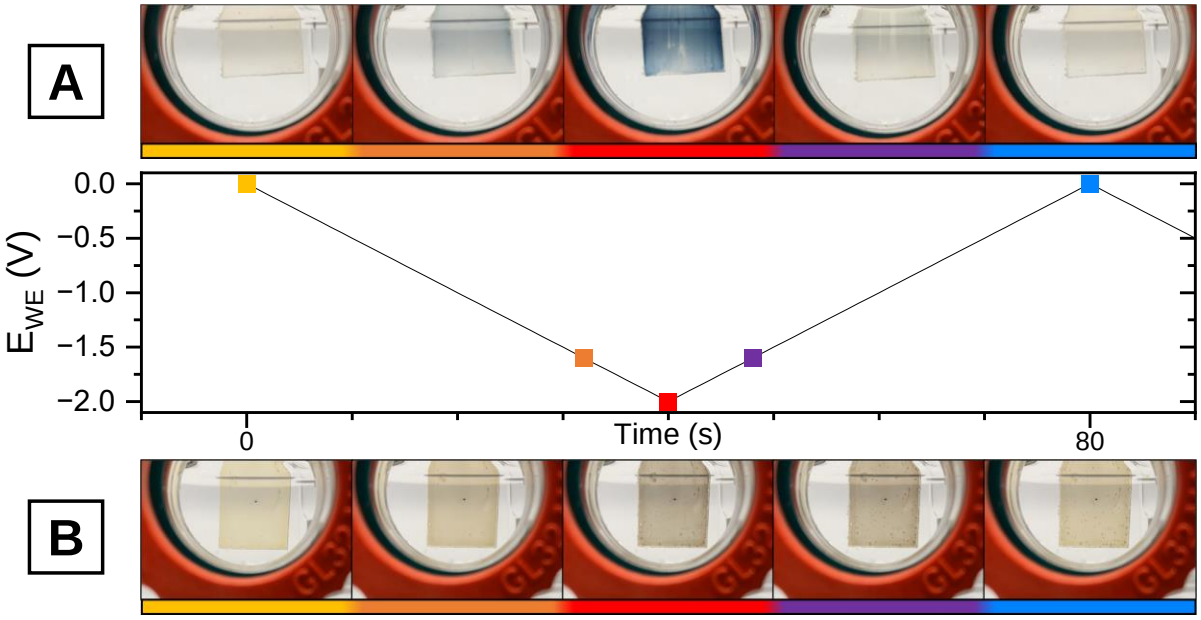

Figure S14 Color change of the thin films during the CV measurements, with the video snapshots corresponding to the applied voltage indicated by color. (A): TiO_2. Yellow: 0 V, start of the measurement. Orange: approximately -1.6 V, slight discoloration to light blue. Red: -2 V, bright blue color. Purple: approximately -1.6 V, reversal of the color change to slight discoloration. Blue: 0 V, color changed back to visibly indistinguishable from the start. (B) NiS@TiO_2: Yellow: 0V, start of the measurement. Orange: approximately -1.6 V, slight darkening of the film. Red: -2 V, discoloration to brown and strong bubble evolution. Purple: approximately -1.6 V, thin film lightens again. Blue: 0 V, thin film color remains slightly darker than prior to the measurement.

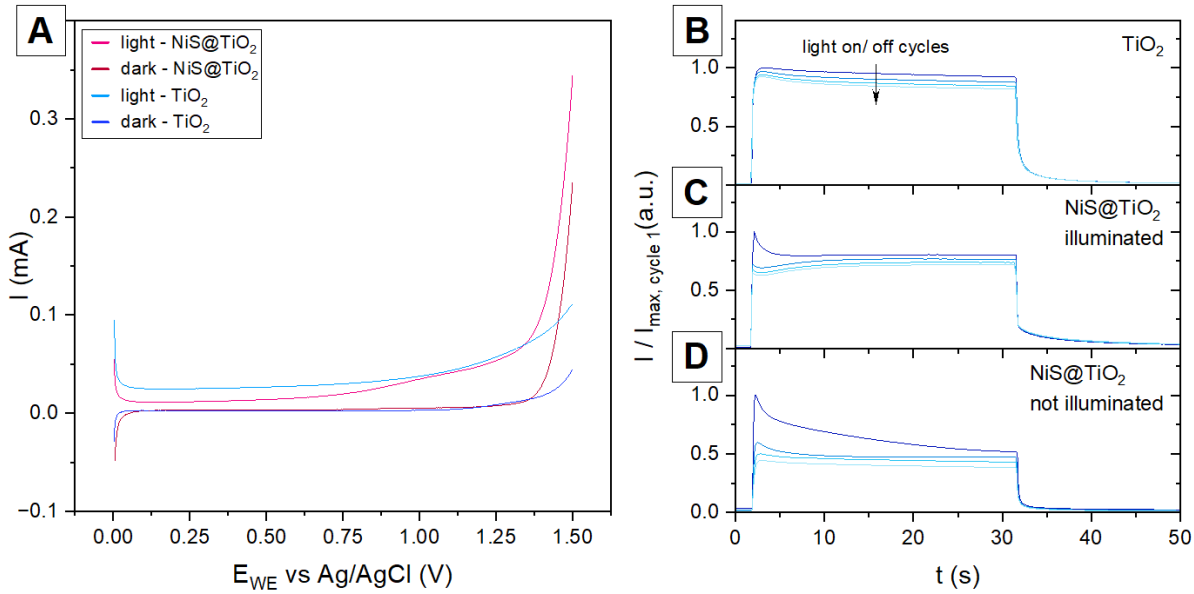

Figure S15 Photoelectrochemical characterizations of TiO_2 and NiS@TiO_2 in 1 M $NaSO_4$. (A) Linear sweep voltammetry from 0 to 1.5 V in dark conditions and under illumination. (B) Manual light-on-off transients for TiO_2, NiS@TiO_2 (preconditioned by illumination in 50 % MeOH) and NiS@TiO_2. For each sample the first four light-on-off cycles are given normalized by the maximum current of the first illumination cycle (dark blue).

For the photoelectrochemical investigations given in Figure S15, some sample was scraped off the thin film catalysts, dispersed in 1 w% aqueous Nafion solution, drop coated onto FTO and dried at 50°C. The light-on-off transients for TiO_2 (Figure S15B), NiS@TiO_2 (Figure S15C, preconditioned by one hour illumination submerged in 50 % MeOH) and pristine NiS@TiO_2 (Figure S15D) are given in Figure 15B. For TiO_2, there is no current “spike” observed upon start of illumination under the applied conditions,

but rather a slightly rounded rise, which might be caused by slow charge transport. This is followed by a slight decrease of the current over time caused by charge carrier recombination. In contrast, for the NiS@TiO_2 samples a pronounced current spike is observed in the first cycle, which decreases in intensity in the following cycles (Figure S15D). We suggest that the decrease and disappearing of this spike can be attributed to some kind of surface conditioning occurring in the catalyst. For the NiS@TiO_2 sample preconditioned by illumination, the difference between the first and second illumination cycle is much lower, and no spike is visible after the first cycle.

X-ray photoelectron spectroscopy (XPS)

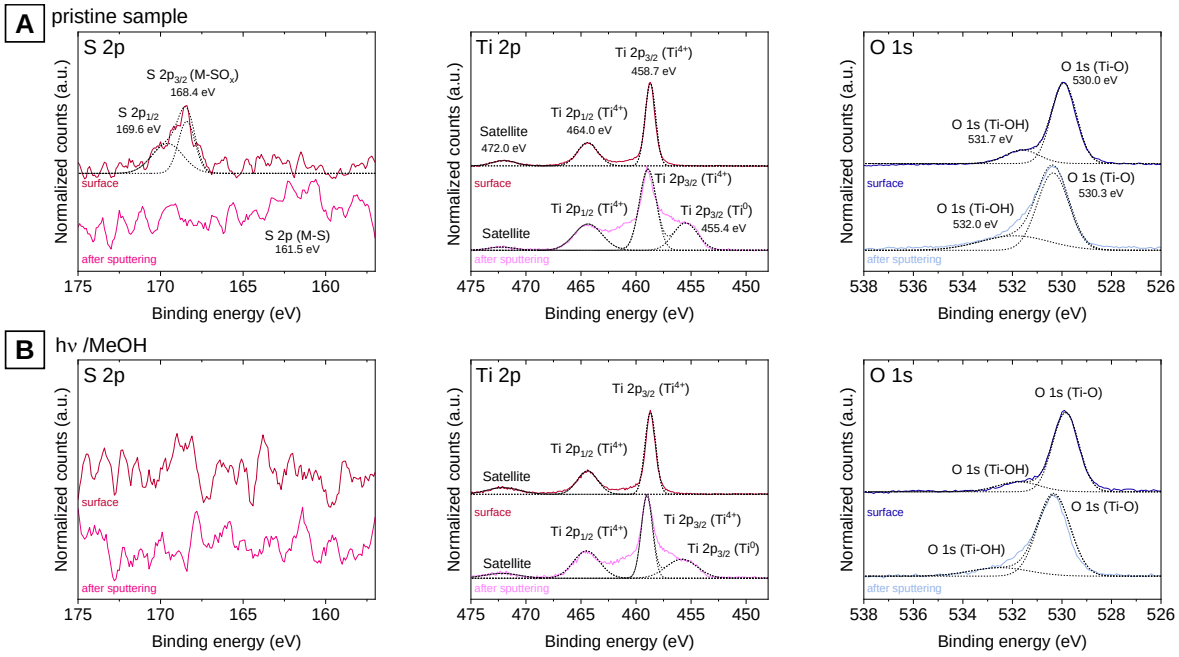

Figure S16 XPS data of (A) an untreated NiS@TiO_2 film and (B) a NiS@TiO_2 film after UV illumination in water/MeOH solution, both films were prepared on a glass/FTO support. For both samples, spectra before and after sputtering of the sample surface are shown. For the S2p spectra, the surface measurement shows a signal corresponding to a metal sulfate species (approx. 168.5 eV). The asymmetric peak shape is a result of the resolution not being sufficient to resolve the closely spaced (1.16 eV) S $2p_{3/2}$ and S $2p_{1/2}$ spin-orbit components. After sputtering, this peak disappears and a low signal for the metal sulfide species emerges (approx. 162 eV).[5] For the Ti 2p spectra, the surface measurements shows the two symmetrical Ti $2p_{3/2}$ and Ti $2p_{1/2}$ peaks at 458.7 and 464.4 eV, respectively. The splitting value of 5.7 eV between the spin-orbit components is characteristic for TiO_2. In the measurement after sputtering an additional signal at a lower energy can be observed, which can be attributed to metallic Ti formed during the sputtering.[6] In the O 1s spectra, next to the main signal corresponding to Ti-O, a small peak at a slightly higher energy is visible, which can be assigned to hydroxylated TiO_2.[7]

Table S2 Comparison of hydrogen evolution rates for different NiS@TiO_2, metal sulfide@TiO_2 / suspension, and metal sulfide@TiO_2 / thin film systems.

Photocatalyst system Thin film (TF) / suspension (S)			**Sacrificial reagent**	**Light source**	**H_2 production** [mmol h^{-1} g^{-1}]	**Year**	**Reference**	**AQE**
NiS@TiO_2	NiS@TiO_2	TF	50 % (v/v) MeOH aq.	365 nm	3.3	2025	This work	0.41
	NiS@TiO_2	S	30 % (v/v) lactic acid	300 W Xe lamp	0.648	2012	Zhang et al.[8]	n.m.
	NiS@TiO_2	S	50 % (v/v) MeOH aq.	500 W Xe lamp	7 ◊	2014	Wang et al.[9]	n.m.
	NiS@TiO_2	S	20 % (v/v) MeOH aq.	350 W Xe lamp	0.655	2018	Xu et al.[10]	n.m.
Suspension systems	Pt@TiO_2		25 % (v/v) EtOH aq.	350 W Xe lamp	16.7 ◊◊	2010	Yu et al.[11]	n.m.
	CdS@TiO_2		0.1 M Na_2S/ 0.1 Na_2SO_4	300 W Xe lamp	4.65	2019	Wu et al.[12]	n.m.
	CdS@TiO_2/Ni_2P				7.42			n.m.
	Pd@TiO_2		25 % (v/v) MeOH aq.	Direct sunlight	35•	2019	Nalajala et al.[13]	0.31
	MoS_2@TiO_2		20 % (v/v) MeOH aq.	365 nm	2.443	2019	Wang et al.[14]	n.m.
	Pt@TiO_2 NTs		5 % (v/v) glycerol aq.	Direct sunlight	173	2019	Lakshmanareddy et al.[15]	n.m.
	CoP_x@TiO_2		20 % (v/v) MeOH aq.	300 W Xe lamp	0.824	2021	Liang et al.[16]	0.7
	CoS_2@TiO_2		25 % (v/v) MeOH / simulated sea water	300 W Xe lamp	9.87	2024	Shanmugaratnam et al.[17]	n.m.
	NiS_2@TiO_2				12.47			n.m.
	SnS_2@TiO_2				2.51			n.m.
Thin film systems	MoS_2@TiO_2		20 % (v/v) MeOH aq.	300 W Xe lamp	580 ••	2018	Guo et al.[18]	n.m.
	Pd@TiO_2		25 % (v/v) MeOH aq.	Direct sunlight	104	2019	Nalajala et al.[13]	0.96
	Cu-Ni(1:1)@TiO_2		25 % (v/v) MeOH aq.	300 W Xe lamp	41.7	2020	Tudu et al.[19]	0.39
	Pt@TiO_2		50 % (v/v) MeOH aq.	13 W UV lamp	0.3496	2023	Mendez et al.[20]	n.m.
	MoP/CdS@TiO_2		10 % (v/v) lactic acid	300 W Xe lamp	35.5	2024	Wang et al.[21]	n.m.
	Pt@TiO_2/PHBH □		10 % (v/v) EtOH aq.	365 nm	90 □	2024	Tasbihi et al.[22]	n.m.
	CdS@TiO_2(anatase) @TiO_2 (rutile)		0.25 M Na_2S/ 0.35 M Na_2SO_3	Direct sunlight	57.95 □□	2026	Banerjee et al.[23]	2.32

◊ reported as 350 µmol h^{-1} for 50 mg catalyst

◊◊ reported as 333.5 µmol h^{-1} for 20 mg catalyst

• read out from the figure + reported as a third of the thin-film efficiency

•• reported normalized to the mass of MoS_2 (30.6 µg cm^{-2}), activity normalized to the mass of total catalyst (MoS_2@TiO_2) was not stated

□ PHBH: poly(hydroxybutyrate-co-hydroxyhexanoate) for immobilization of TiO_2

□□ reported as 57.95 µmol h^{-1} for 1 mg catalyst

Table S3 Prices of different metals for 24.10.2025

Metal	**Price [$]**	**Price [€ kg^{-1}]**
Ni[24]	15323.9 / ton	13.0
Pd[25]	1463.7 / oz	39 844
Pt[26]	1593.7 / oz	43 383

References

1 A. R. Hind and L. Chomette, *The determination of thin film thickness using reflectance spectroscopy (Publication Number SI-A-1205)*, Agilent Technologies Inc., 2011.

2 P. Karasiński, E. Gondek, S. Drewniak and I. V. Kityk, *J. Sol-Gel Sci. Technol.*, 2012, **61**, 355–361.

3 K. R. Phillips, T. Shirman, M. Aizenberg, G. T. England, N. Vogel and J. Aizenberg, *J. Mater. Chem. C*, 2020, **8**, 109–116.

4 G. Yin, X. Huang, T. Chen, W. Zhao, Q. Bi, J. Xu, Y. Han and F. Huang, *ACS Catal.*, 2018, **8**, 1009–1017.

5 M. Lu, N. Gao, X.-J. Zhang and G.-S. Wang, *RSC Adv.*, 2019, **9**, 5550–5556.

6 P. Bargiela, V. Fernandez, D. Morgan, M. Richard-Plouet, N. Fairley and J. Baltrusaitis, *Results Surf. Interfaces*, 2024, **15**, 100231.

7 C. Fan, C. Chen, J. Wang, X. Fu, Z. Ren, G. Qian and Z. Wang, *Sci. Rep.*, 2015, **5**, 11712.

8 L. Zhang, B. Tian, F. Chen and J. Zhang, *Int. J. Hydrogen Energy*, 2012, **37**, 17060–17067.

9 Q. Wang, G. Yun, Y. Bai, N. An, Y. Chen, R. Wang, Z. Lei and W. Shangguan, *Int. J. Hydrogen Energy*, 2014, **39**, 13421–13428.

10 F. Xu, L. Zhang, B. Cheng and J. Yu, *ACS Sustain. Chem. Eng.*, 2018, **6**, 12291–12298.

11 J. Yu, L. Qi and M. Jaroniec, *J. Phys. Chem. C*, 2010, **114**, 13118–13125.

12 K. Wu, P. Wu, J. Zhu, C. Liu, X. Dong, J. Wu, G. Meng, K. Xu, J. Hou, Z. Liu and X. Guo, *Chemical Engineering Journal*, 2019, **360**, 221–230.

13 N. Nalajala, K. K. Patra, P. A. Bharad and C. S. Gopinath, *RSC Adv.*, 2019, **9**, 6094–6100.

14 W. Wang, S. Zhu, Y. Cao, Y. Tao, X. Li, D. Pan, D. L. Phillips, D. Zhang, M. Chen, G. Li and H. Li, *Adv. Funct. Materials.*, 2019, **29**, 1901958.

15 N. Lakshmanareddy, V. Navakoteswara Rao, K. K. Cheralathan, E. P. Subramaniam and M. V. Shankar, *Journal of Colloid and Interface Science*, 2019, **538**, 83–98.

16 R. Liang, Y. Wang, C. Qin, X. Chen, Z. Ye and L. Zhu, *Langmuir*, 2021, **37**, 3321–3330.

17 S. Shanmugaratnam, P. Ravirajan, Y. Shivatharsiny and D. Velauthapillai, *Int. J. Hydrogen Energy*, 2024, **91**, 673–682.

18 L. Guo, Z. Yang, K. Marcus, Z. Li, B. Luo, L. Zhou, X. Wang, Y. Du and Y. Yang, *Energy Environ. Sci.*, 2018, **11**, 106–114.

19 B. Tudu, N. Nalajala, P. Saikia and C. S. Gopinath, *Solar RRL*, 2020, **4**, 1900557.

20 F. J. Méndez, D. Barrón-Romero, O. Pérez, R. D. Flores-Cruz, Y. Rojas-Challa and J. A. García-Macedo, *Materials Chemistry and Physics*, 2023, **305**, 127925.

21 J. Wang, J. Tian, P. Han, L. Song, W. Wang, K. Lin, D. Feng and B. Ma, *Langmuir*, 2024, **40**, 21161–21170.

22 M. Tasbihi, S. Kwon, B. Kim, D. Brüggemann, H. Hou, J. Lu, R. Amitrano, T. Grimm, J. García-Antón, P. Strasser, S. L. Riedel and M. Schwarze, *Langmuir*, 2024, **40**, 25800–25810.

23 N. Banerjee, A. Roy and R. G. Nair, *Fuel*, 2026, **406**, 136920.

24 Trading Economics, Nickel, https://tradingeconomics.com/commodity/nickel, (accessed October 24, 2025).

25 Trading Economics, Palladium, https://tradingeconomics.com/commodity/palladium, (accessed February 4, 2026).

26 Trading Economics, Platinum, https://tradingeconomics.com/commodity/platinum, (accessed October 24, 2025).